Title

Reliability of two-dimensional and three-dimensional pseudo-continuous arterial spin labeling perfusion MRI in elderly populations: Comparison with 15o-water positron emission tomography

Journal

Journal of Magnetic Resonance Imaging, 39(4)

ISSN

1053-1807

Authors

Kilroy, Emily
Apostolova, Liana
Liu, Collin
et al.

Publication Date

2014-04-01

DOI

10.1002/jmri.24246

Peer reviewed

Original Research

Reliability of Two-Dimensional and Three-Dimensional Pseudo-Continuous Arterial Spin Labeling Perfusion MRI in Elderly Populations: Comparison With 15O-Water Positron Emission Tomography

Emily Kilroy, MS,[1] Liana Apostolova, MD,[1,2] Collin Liu, MD,[1,3] Lirong Yan, PhD,[1] John Ringman, MD,[1,2] and Danny J.J. Wang, PhD, MSCE[1]*

Purpose: To investigate the reliability and accuracy of two pseudo-continuous arterial spin labeling (pCASL) sequences, using two-dimensional (2D) gradient-echo echo planar imaging (EPI) and 3D gradient and spin echo (GRASE) as the readout, respectively.

Materials and Methods: Each sequence was performed twice 4 weeks apart on six normal control subjects, six elderly subjects with mild cognitive impairment (MCI), and one participant with Alzheimer's disease (AD). Eight of these subjects also underwent $H_2{}^{15}O$ positron emission tomography (PET) scans on the same day or proximal to their second MRI scan. The longitudinal repeatability of EPI and GRASE pCASL were evaluated with the intraclass correlation coefficient (ICC) and within-subject coefficient of variation (wsCV).

Results: The ICCs of global perfusion measurements were 0.697 and 0.413 for GRASE and EPI based pCASL respectively. GRASE pCASL also demonstrated a higher longitudinal repeatability for regional perfusion measurements across 24 regions-of-interests (ICC = 0.707; wsCV = 10.9%) compared with EPI pCASL (ICC = 0.362; wsCV = 15.3%). When compared with PET, EPI pCASL showed a higher degree of spatial correlation with PET than GRASE pCASL, although the difference was not statistically significant.

Conclusion: The 3D GRASE pCASL offers better repeatability than 2D EPI pCASL, thereby may provide a reliable imaging marker for the evaluation of disease progression and treatment effects in MCI and early AD subjects.

Key Words: cerebral blood flow (CBF); perfusion; arterial spin labeling (ASL); echo planner imaging (EPI); gradient and spin echo (GRASE); Alzheimer's disease (AD); magnetic resonance imaging (MRI); positron emission tomography (PET)
J. Magn. Reson. Imaging 2014;39:931–939.

ALZHEIMER'S DISEASE (AD) affects more than 35 million people worldwide, 5.5 million in the United States, and causes tremendous social economical burden. The focus of treatment development for AD is to halt or change the disease process before neurons are irreversibly damaged. Evaluation of these potential treatments will benefit from brain imaging techniques that can identify patients at the earliest stages of the disease and can objectively measure disease progression. Amyloid deposition, detectable by positron emission tomography (PET), is one of the earliest pathological events in AD, but studies have shown that the level of deposition does not correlate well with cognitive decline (1,2). Brain atrophy detected using structural MRI represents relatively late changes in the AD process (3). Functional and metabolic imaging markers such as cerebral blood flow (CBF) and cerebral metabolic rate of glucose (CMRglc) show progressive changes during the conversion from mild cognitive impairment (MCI) to AD (3,4). Reduced CBF and glucose metabolism have been detected in AD, and to a lesser extent in MCI subjects, using existing nuclear medicine imaging techniques that rely on radioactive tracers.

Arterial spin labeling (ASL) perfusion MRI is an appealing approach for measuring perfusion in dementia by using magnetically labeled arterial blood water as an endogenous tracer. ASL does not involve

[1]Department of Neurology, University of California Los Angeles, Los Angeles, California, USA.
[2]Mary S. Easton Center for Alzheimer's Disease Research, University of California Los Angeles, Los Angeles, California, USA.
[3]Department of Neurology, University of Southern California, Los Angeles, California, USA.
Contract grant sponsor: NIH; Contract grant number: R01-MH080892; Contract grant number: R01-NS081077; Contract grant number: R01-AG040770; Contract grant number: R01-EB014922; Contract grant number: P50-AG016570; Contract grant sponsor: the Easton Consortium for Alzheimer's Disease Drug and Biomarker Discovery.
*Address reprint requests to: D.J.J.W., Department of Neurology, University of California Los Angeles, 660 Charles E Young Dr. South, Los Angeles, CA 90095. E-mail: jwang71@gmail.com
Received November 28, 2012; Accepted May 3, 2013.
DOI 10.1002/jmri.24246
View this article online at wileyonlinelibrary.com.

Table 1
Demographic and Behavioral Evaluation Information of Participants

	Gender	Age	Diagnosis	MMSE	CDR-SOB
MRI	M = 9, F = 4	Avg = 68, SD = 5.85	NC = 6	NC = 28	NC = .083
N = 13		Range = 57–78	MCI = 6	MCI = 28	MCI = .75
			AD = 1	AD = 20	AD = 8.5
PET	M = 4, F = 4	Avg = 67, SD = 6.51	NC = 3	NC = 28	NC = .167
N = 8		Range = 57–78	MCI = 4	MCI = 27	MCI = .75
			AD = 1	AD = 20	AD = 8.5

radiation or contrast agents, allows easy registration with structural MRI, and provides absolute CBF that has been shown to be reproducible across time scales from minutes, hours, to days (5,6). To date, several groups have applied ASL to study AD and MCI. Characteristic patterns of cerebral hypoperfusion in temporoparietal association cortices, posterior cingulate cortex (PCC), and frontal cortex were detected using ASL in AD patients, and to a lesser extent, in MCI populations (7–10) (see review (4) for details). Of interest, hyperperfusion in basal ganglia, amygdala, and hippocampus have been reported in MCI and mild AD subjects, after effects of brain atrophy on CBF were adjusted (9,11). Based on these pilot studies, ASL is beginning to be accepted by the AD community as a promising imaging tool for monitoring disease progression in MCI and AD.

The reliability of ASL perfusion measurement has been assessed by several studies in typically young, healthy adult populations (6,12–14). To date, besides a small study conducted in six elderly subjects (15), few studies have systematically and rigorously addressed the longitudinal repeatability and accuracy of ASL in elderly populations at risk for or diagnosed with dementia. Elderly populations may pose unique challenges for ASL because the signal to noise ratio (SNR) is likely reduced with potential vascular changes compared with younger populations. The primary purpose of the present study was therefore to establish the test–retest repeatability of pseudo-continuous ASL (pCASL) using repeated MRI scans approximately 4 weeks apart in a cohort of MCI, AD subjects and age matched controls. In addition, the accuracy of pCASL perfusion MRI was assessed by comparison with the gold standard of CBF measurement using 15O-water PET, which was conducted on the same day or proximal to the second MRI scan.

A recent trend in ASL development is the use of fast three-dimensional (3D) sequences such as GRASE and SPIRAL, often in conjunction with background suppression, to improve the SNR and reliability of ASL perfusion measurements (16,17). In the present study, both 2D gradient-echo EPI based pCASL and 3D GRASE pCASL with background suppression (BS) were performed for comparison. We hypothesized that 3D GRASE pCASL will show improved test–retest reproducibility compared with 2D EPI based pCASL.

MATERIALS AND METHODS

Participants

A total of 14 participants were recruited and clinically assessed. All subjects provided written informed consent, which were approved by the Institutional Review Board and the Medical Radiation Safety Committee of the University. Thirteen participants completed 2 repeated MRI scans and were included in the analysis. They included six normal controls (NC, 5 male), six MCI (3 male), and one AD subject (male). Subjects were all over 55 years of age with a mean age of 68 (SD = 5.85). All participants were sufficiently fluent in English and in good general health. The Mini Mental State Exam (MMSE) and the Clinical Dementia Rating Sum of Boxes (CDR-SOB) were performed on each participant (see Table 1 for detailed demographic and behavioral testing scores). Study exclusion criteria included contraindications to MRI and PET, history of major head trauma, other concurrent neurologic or psychiatric illnesses, and abnormal structural MRI. Excluded medications included short or long acting nitrates, and warfarin or other drugs that may affect CBF (such as caffeine within 3 h and nicotine within 1 h of the imaging exam).

Pseudo-Continuous Arterial Spin Labeling MRI

Each subject underwent two MRI scans approximately 4 weeks apart on a 3 Tesla (T) Siemens TIM Trio scanner, using body coil as the transmitter and 12-channel head coil as the receiver. Each MRI included a 3D MPRAGE sequence for T1-weighted structural MRI with the following specifications: 192 slices at 1-mm slice thickness, voxel size: $1.0 \times 1.0 \times 1.0$ mm^3, field of view (FOV) = 256 mm, flip angle = 9°, repetition time (TR) = 1900 ms, echo time (TE) = 3.25 ms, rate-2 GRAPPA for a total scan time of 4 min 30 s. Two pCASL sequences were performed: (i) 2D EPI pCASL with the following parameters: FOV = 220 mm, matrix = 64×64, TR/TE = 4000/11 ms, rate-2 GRAPPA, 24 5-mm slices with a 1-mm gap in the transverse orientation acquired from inferior to superior direction (35 ms per slice), postlabeling delay (PLD) = 1500 ms, 40 pairs of label and control acquisitions with a total scan time of 5min 20 s; (ii) 3D GRASE pCASL with the following parameters: FOV = 220 mm, matrix = 64×64, TR/TE = 4000/22 ms, rate-2 GRAPPA in phase, 4/8 partial *k*-space in slice direction, 26 5-mm slices with 7% oversampling rate, PLD = 1500 ms during which two nonselective inversion pulses were applied for BS, 30 pairs of label and control acquisitions with a total scan time of 4 min. Although the acquisition was shorter for GRASE than EPI, the SNR of GRASE images was 40% higher than that of EPI. A M_0 image was acquired with a TR of 5 s and without labeling pulses for 3D GRASE pCASL. For 2D EPI

pCASL, the control image was used as M_0 because no background suppression was applied. In both sequences, an radiofrequency pulse train of 1500-ms duration was applied 9 cm beneath the center of the acquired slices, with a mean gradient of 0.6 mT/m, and a maximum gradient of 6 mT/m (16,18).

CBF Calculations

ASL images were corrected for motion, pairwise subtracted between label and control images followed by averaging to generate the mean difference image (ΔM). Quantitative CBF (f) maps were calculated based on the following equation (18)

$$f = \frac{\lambda \Delta M R_{1a}}{2\alpha M_0 [\exp(-\omega R_{1a}) - \exp(-(\tau + \omega) R_{1a})]}, \quad [1]$$

where R_{1a} (0.61 s^{-1}) is the longitudinal relaxation rate of blood, M_0 is the equilibrium magnetization of brain tissue, α (=0.85 for EPI, 0.77 to account for loss of efficiency by BS for GRASE) is the tagging efficiency (19), τ (=1.5 s) is the duration of the labeling pulse, ω (=1.5 s) is the postlabeling delay time (slice acquisition time was adjusted for 2D EPI) and λ (=0.9 g/mL) is blood/tissue water partition coefficient. Equation [(1)] assumes that the labeled blood spins remain primarily in the vasculature rather than exchanging completely with tissue water, which is justified in elderly subjects in whom arterial transit times are likely prolonged (20).

Each ASL MRI scan was co-registered (using EPI and GRASE images, respectively) to the T1-weighted structural MRI, and normalized to the Montreal Neurological Institute template (MNI) with Statistical Parametric Mapping (SPM8) Software (www.fil.ion.ucl.ac.uk/spm8) using the nonlinear normalization function with preserving concentration option. All images were smoothed with a 4-mm full width half maximum (FWHM) Gaussian kernel filter after normalization.

PET

Eight subjects also participated in one PET scan using the whole body ECAT EXACT HR+ Siemens PET Scanner. Subjects were given a physical exam by a physician to determine if the participant was healthy for the scan. If determined eligible (blood pressure below 140/90 mmHg and good physical and mental health), subjects underwent $H_2{}^{15}O$ PET scan the same day or shortly after their second MRI scan. Six subjects received a PET scan the same day as their last MRI, and two subjects were scanned within 2 weeks after their second MRI (3 and 13 days later). During both MRI and PET scans, subjects were instructed to rest quietly with eyes closed.

For $H_2{}^{15}O$ PET, 10–15 mCi of 15O-water was injected as a rapid bolus (<5 s). A series of dynamic frames were acquired for a total of 2 min following injection, and 3–4 injections were performed in each subject with a 10-min break between each. Sixty-three slices in the axial plane were obtained with a resolution of 1.8 mm × 1.8 mm × 2.4 mm (matrix = 128 × 128). PET data were reconstructed using filtered back projection with corrections for attenuation and scatter. No arterial sampling was performed and relative CBF (rCBF) images were generated by averaging the dynamic frames in each scan with correction of tracer decay. A mean rCBF map was then calculated by averaging the three to four injections. Mean rCBF maps were normalized to the MNI space using the PET template provided by SPM8 and smoothed with a 4-mm FWHM Gaussian kernel. In each subject, PET rCBF maps were scaled so that the global mean CBF was 50 mL/100 g/min to adjust the variations in tracer dosage across subjects.

Statistical Analysis

For each subject, normalized structural MRI were segmented into gray matter (GM), white matter (WM), and cerebrospinal fluid compartments using SPM8. The GM and WM segmentations were combined to form a brain tissue mask. Mean ASL and PET CBF values were extracted from GM, WM, and whole brain masks, as well as from 90 regions of interest (ROIs) defined by the Automated Anatomical Labeling (AAL) template (21).

The test–retest reliability of pCASL scans were evaluated with the classic intraclass correlation coefficient (ICC) and within-subject coefficient of variation (wsCV) using the SPSS software package (Chicago, IL). Separate comparisons were performed to evaluate test–retest reliability for GM, WM, and whole brain (WB) CBF in all subjects between time-point 1 (Scan 1) and time-point 2 (Scan 2). Bland-Altman plots were generated to display the spread of data and to evaluate the measurement agreement between Scan 1 and 2 for whole brain, GM and WM mean CBF respectively. ICC and wsCV were also calculated for mean CBF values in 90 ROIs of the AAL template. Special attention was paid to 24 specific ROIs that have previously been reported to be implicated in MCI and AD (4). These regions included bilateral posterior cingulate, hippocampus, superior and inferior parietal, precuneus, parahippocampal, amygdala, superior temporal gyrus, fusifrom gyrus, lingual gyrus, supramarginal and angular gyrus. ICC and wsCV values of GRASE and EPI pCASL were compared using the Wilcoxon signed-rank test across the 24 ROIs. Within-subject analysis of variance (ANOVA) was used to compare mean CBF values acquired using GRASE and EPI pCASL in GM, WM, and WB, respectively. Furthermore, accuracy was determined by comparing MRI CBF measurements with PET CBF measurements across the 90 ROIs of the AAL template as well as across all brain pixels in each subject, using Pearson correlation coefficients.

Based on the mean variability of CBF measurements (wsCV) across 24 ROIs, power calculations were performed to determine the number of subjects (N) required to detect a given effect size for GRASE and EPI pCASL, respectively (14). The *sampsi* function with the *ancova* method provided by the STATA 10.0 software (College Station, TX) was used for the

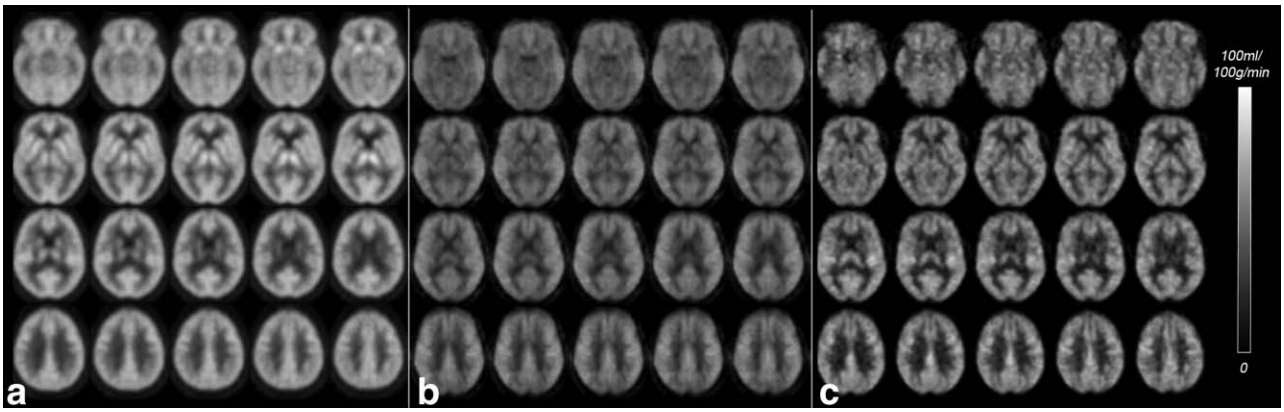

Figure 1. Average CBF maps of the 8 subjects participating in both PET and MRI experiments: PET (**a**), pCASL GRASE (**b**), and pCASL EPI (**c**). PET rCBF maps were scaled to a global mean CBF value of 50 mL/100 g/min.

calculation, assuming a conservative correlation coefficient of 0.25 to 0.5 between repeated measurements.

RESULTS

Subjects

Table 1 lists the demographic and clinical information of the 13 participants with their MMSE and CDR SOB scores. When split into clinical and nonclinical groups, participants did not differ in age ($P = 0.334$), MMSE ($P = 0.275$), or CDR SOB scores ($P = 0.178$), based on Wilcoxon rank-sum test.

Qualitative Comparison of CBF Maps

Eight participants underwent pCASL EPI and pCASL GRASE MRI scans as well as $H_2{}^{15}O$ PET scans. The mean normalized CBF maps of the eight participants for each technique are illustrated in Figure 1. Qualitatively, CBF maps obtained by the three techniques are comparable and show good contrast between GM and WM. Nevertheless, the GRASE CBF map has lower CBF values than those of EPI which is elaborated below.

Test–Retest Repeatability

Thirteen participants underwent repeated MRI scans. PCASL EPI and pCASL GRASE showed moderate (ICC = 0.4–0.6) to good (ICC = 0.6–0.8) levels of test–retest reproducibility between repeated MRIs acquired 4 weeks apart. As summarized in Table 2, pCASL GRASE produced higher ICC values compared with pCASL EPI in GM, WM, and whole brain. The wsCV values were also reduced in GRASE pCASL compared with EPI pCASL, especially for WM CBF measurements. The above observation is further illustrated in Figure 2 of the Bland-Altman plots. The differences between two repeated scans were generally distributed within ±(10–15) mL/100 g/min (or ±2SD) in GRASE pCASL, while they were distributed within approximately ±20 mL/100 g/min in EPI pCASL across GM, WM, and whole brain. However, GRASE pCASL CBF measurement demonstrated a small negative bias (<5 mL/100 g/min, n.s.) between the two repeated scans.

A similar pattern emerged when examining the reliability of CBF measurements across the 24 ROIs relevant to the progression of AD (see Table 3). The mean ICC across the 24 representative ROIs was 0.707 and 0.362, and the mean wsCV 10.9 and 15.3% for GRASE and EPI based pCASL, respectively. The Wilcoxon signed-rank test indicated significantly higher ICC ($P < 0.001$) and reduced wsCV ($P < 0.001$) using GRASE compared with EPI pCASL.

Quantitative CBF Measurements

The mean CBF values measured by EPI and GRASE pCASL in GM, WM, and whole brain are displayed in Figure 3. Consistent with Figure 1, the mean CBF values were reduced in GM ($F(1,11) = 55.4$, $P < 0.001$) and whole brain ($F(1,11) = 16.9$, $P < 0.001$) in GRASE pCASL compared with EPI pCASL, based on within-subject ANOVA. In contrast, WM CBF was significantly greater in GRASE pCASL compared with EPI pCASL ($F(1,11) = 28.1$, $P < 0.001$).

Comparison Between ASL and PET

The accuracy of pCASL CBF measurements was determined by correlating the second pCASL CBF

Table 2
Test-Retest Results of Mean CBF (mL/100 g/min) in Gray Matter, White Matter, and Whole Brain Using 2D EPI- and 3D GRASE-Based pCASL

	EPI				GRASE			
	CBF scan 1	CBF scan 2	ICC	CV	CBF scan 1	CBF scan 2	ICC	CV
Gray matter	54.33 ± 10.84	54.72 ± 8.99	0.404	0.102	48.02 ± 10.37	52.33 ± 9.95	0.718	0.099
White matter	25.75 ± 7.85	25.16 ± 10.50	0.424	0.256	31.56 ± 7.90	33.55 ± 7.30	0.623	0.117
Whole brain	47.58 ± 9.96	48.01 ± 8.45	0.413	0.106	43.29 ± 9.55	47.20 ± 8.43	0.697	0.103

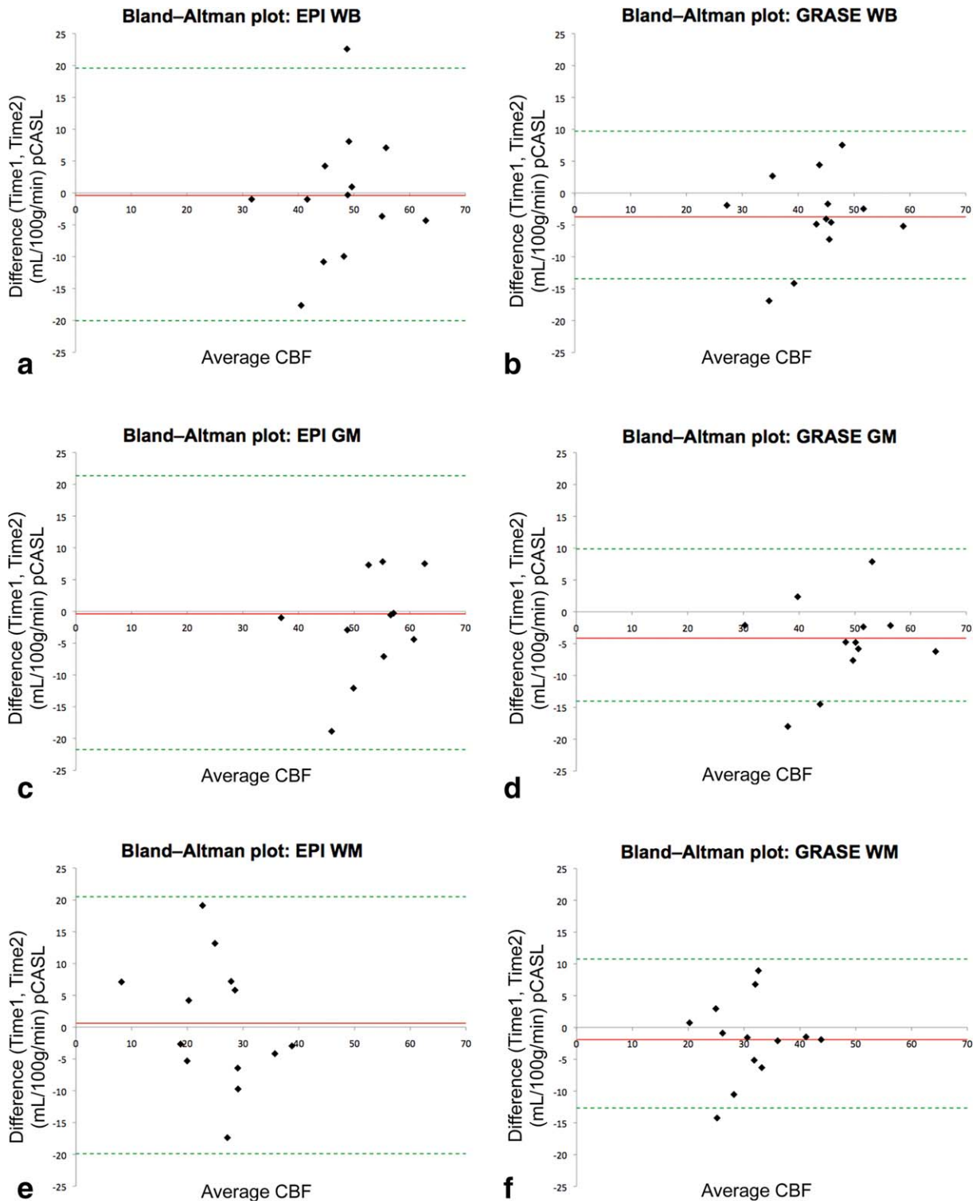

Figure 2. Bland-Altman plots of repeated CBF measurements using EPI pCASL (**a,c,e**) and GRASE pCASL (**b,d,f**) in whole brain (WB) (a,b), gray matter (GM) (c,d), and white matter (WM) (e,f), respectively.

(Scan 2) and PET rCBF measurements across 90 ROIs of the AAL template as well as across all brain pixels in each subject. Representative ASL CBF and PET rCBF images from a 65-year-old subject (female, MCI) are shown in Figure 4. GRASE pCASL maps show higher SNR while EPI pCASL maps show higher contrast between GM and WM. Statistically significant associations between pCASL CBF and PET rCBF were found for both GRASE and EPI sequences in ROI and pixel-wise correlations. When comparing mean CBF values across 90 AAL ROIs, pCASL EPI showed higher correlations with PET rCBF compared with pCASL GRASE (pCASL EPI: r = 0.51; SD = 0.11; $P < 0.001$; pCASL GRASE r = 0.40; SD = 0.13; $P < 0.001$). Figure 5 displays the correlation coefficients across the 8 participants. However, such difference between

Table 3
Test-Retest Results of EPI and GRASE pCASL Across 24 Representative ROIs

	EPI CBF (mL/100 g/min)				GRASE CBF (mL/100 g/min)			
	Scan 1 Mean	Scan 2 Mean	ICC	wsCV	Scan 1 Mean	Scan 2 Mean	ICC	wsCV
Cingulum_Post_L	60.78	61.21	0.386	0.153	53.86	58.62	0.533	0.139
Cingulum_Post_R	46.90	49.68	−0.010	0.216	47.55	50.35	0.440	0.124
Hippocampus_L	47.13	49.65	0.306	0.167	38.81	42.98	0.784	0.096
Hippocampus_R	47.08	46.98	0.365	0.145	40.30	44.24	0.698	0.091
ParaHippocampal_L	39.85	40.91	0.380	0.136	37.06	40.83	0.745	0.094
ParaHippocampal_R	41.90	44.30	0.323	0.155	39.90	43.42	0.773	0.081
Amygdala_L	42.71	47.55	0.090	0.203	40.43	44.21	0.771	0.093
Amygdala_R	42.38	39.08	0.219	0.203	40.28	43.08	0.647	0.087
Fusiform_L	47.89	47.19	0.304	0.141	37.52	41.90	0.785	0.107
Fusiform_R	42.12	44.34	0.340	0.138	37.74	41.22	0.639	0.114
Parietal_Sup_L	46.13	48.40	0.534	0.166	37.52	40.50	0.749	0.136
Parietal_Sup_R	40.76	40.05	0.307	0.227	36.54	39.60	0.721	0.127
Parietal_Inf_L	55.55	59.02	0.616	0.153	49.28	53.11	0.756	0.104
Parietal_Inf_R	53.81	55.08	0.377	0.186	46.70	52.98	0.755	0.129
SupraMarginal_L	57.99	61.66	0.460	0.140	54.59	59.56	0.673	0.100
SupraMarginal_R	50.69	50.68	0.109	0.132	49.87	55.11	0.813	0.092
Angular_L	57.92	61.03	0.439	0.133	54.26	58.96	0.751	0.106
Angular_R	54.63	56.44	0.458	0.119	48.78	53.70	0.804	0.111
Precuneus_L	52.68	54.47	0.437	0.148	45.21	49.52	0.612	0.130
Precuneus_R	51.25	52.85	0.338	0.151	45.03	48.36	0.516	0.117
Temporal_Sup_L	59.35	58.44	0.431	0.107	52.11	57.35	0.721	0.102
Temporal_Sup_R	49.35	47.46	0.389	0.135	48.18	52.79	0.875	0.086
Lingual_L	55.21	53.12	0.429	0.122	44.11	47.49	0.644	0.125
Lingual_R	53.06	52.56	0.649	0.092	41.46	45.23	0.771	0.115
Average ± SD	49.88 ± 6.31	50.92 ± 6.68	0.362 ± 0.151	0.153 ± 0.034	44.46 ± 5.96	48.55 ± 6.53	0.707 ± 0.103	0.109 ± 0.017

correlation coefficients of EPI and GRASE CBF was not statistically significant using the Wilcoxon signed-rank test ($P = 0.09$). Similarly, correlation analyses across brain pixels revealed significant associations between EPI and GRASE pCASL vs. PET rCBF (pCASL EPI r = 0.53; SD = 0.06; $P < 0.001$; PET and pCASL GRASE r= 0.51; SD = 0.08; $P < 0.001$, see Fig. 5b). Again there was no significant difference between GRASE and EPI based pCASL scans ($P = 0.40$).

Sample Size Estimation

Figure 6 shows estimated sample size for a within-subject design including one baseline and one follow-up measurement based on the mean wsCV of 10.9 and 15.3% for GRASE and EPI pCASL, respectively. For an expected CBF change of 15%, the sample size is around 10 and 20 for GRASE and EPI pCASL respectively with an assumed correlation coefficient of 0.25–0.5 between repeated measures ($\alpha = 0.05$ two-sided and power = 90%).

DISCUSSION

In the present study, we systematically evaluated the longitudinal reliability of 2 pCASL sequences with 2D EPI and 3D GRASE readout respectively in a cohort of 13 elderly subjects at risk for or diagnosed with AD. The results showed that 3D GRASE pCASL had a higher test–retest repeatability compared with 2D EPI pCASL, as manifested by greater ICC and lower wsCV values using GRASE pCASL for both global and regional perfusion measurements. The interval of approximate 4 weeks between repeated MRI scans represents a "real-world" situation for testing imaging markers in MCI and AD. The observed higher test–retest repeatability using 3D GRASE pCASL compared with 2D EPI pCASL may be attributed to the higher SNR of 3D acquisitions, reduced temporal fluctuations using background suppression, and reduced T1 relaxation of the label due to the single-shot excitation of 3D GRASE (14). In addition, susceptibility effects in orbitofrontal and inferior temporal cortex are reduced

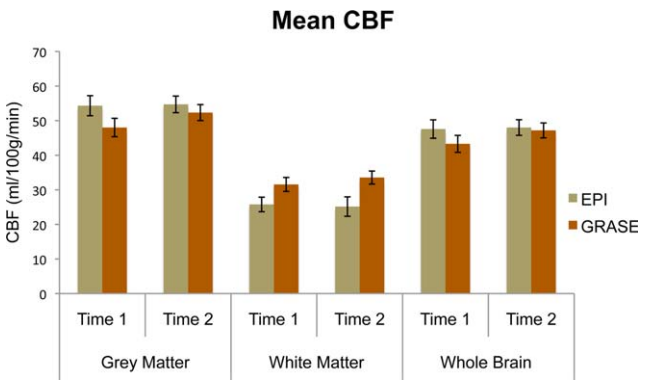

Figure 3. Mean CBF values in GM, WM, and WB acquired using EPI and GRASE based pCASL at two time points, respectively, error bars indicate standard error. [Color figure can be viewed in the online issue, which is available at wileyonlinelibrary.com.]

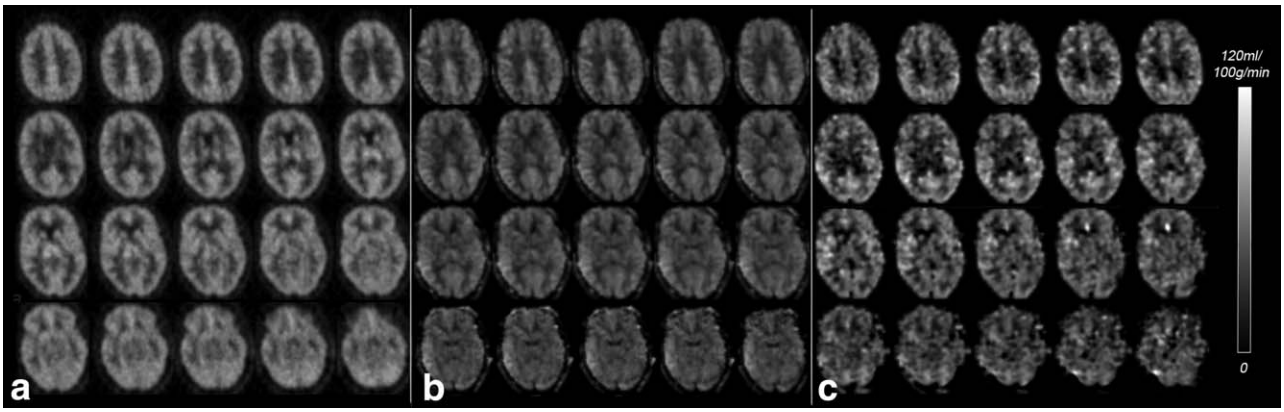

Figure 4. Representative CBF maps of a 65 year old participant (female, MCI) acquired using different techniques: PET (**a**), pCASL GRASE (**b**), and pCASL EPI (**c**). PET rCBF maps were scaled to a global mean CBF value of 50 mL/100 g/min.

using 3D GRASE compared with 2D EPI (22). Based on our data, pCASL with 3D BS GRASE readout should be the method of choice for longitudinal imaging studies to follow disease progression and treatment effects in MCI and mild AD.

One shortcoming of 3D GRASE, however, is the spatial blurring due to modulations of *k*-space signals by the T2 relaxation curve, especially along the z-direction. It has been reported that the readout duration of 3D acquisitions should be less than $\pi T2$ to ensure that blurring is less than the voxel size (23). With a T2 of ~100 ms for GM and a T2 of ~80 ms for WM at 3T, the readout durations for GM and WM should be less than 314 and 251 ms, respectively, to minimize blurring effect. In the present experiment, we used 14 spin echoes along the z-direction (4/8 partial *k*-space) resulting in an echo train length of 350 ms. A small amount of spatial blurring is expected in 3D GRASE pCASL perfusion images. The calculated mean CBF values were significantly lower in GM and higher in WM using GRASE pCASL compared with EPI pCASL, suggesting partial volume effects between grey and white matter using 3D GRASE. Segmented or multi-slab 3D acquisition is an effective approach to minimize spatial blurring, however, at the cost of prolonged scan time. In addition, potential head motion between segmented acquisitions in uncooperative subjects poses a risk for scanning demented or stroke patients (24). An alternative solution to spatial blurring involves the catalyzation of a pseudo-steady state using variable flip angles (VFA) during the echo train

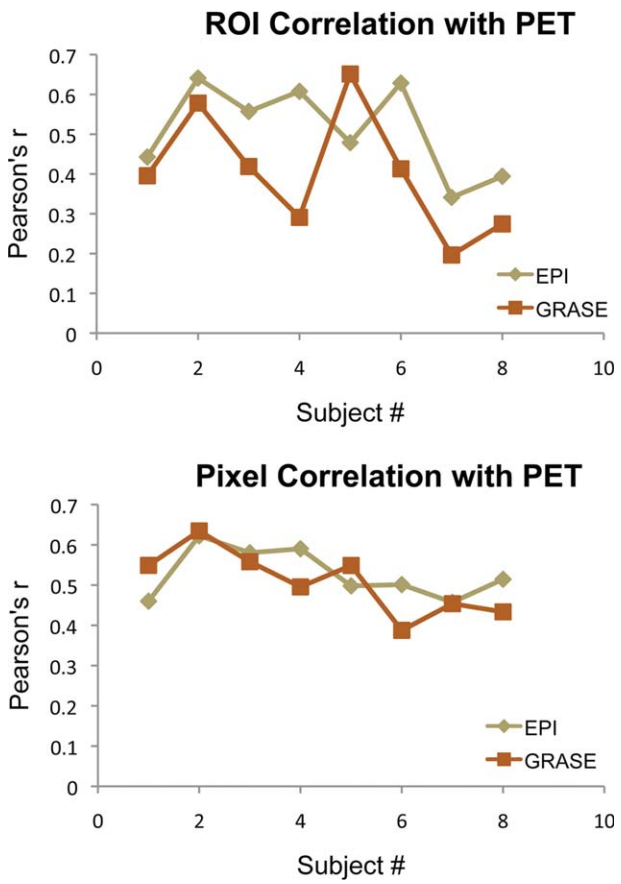

Figure 5. Pearson's correlation coefficients between EPI and GRASE pCASL versus PET rCBF across 90 ROIs of the AAL template (**a**), as well as across all brain pixels (**b**) in the eight subjects participating in both PET and MRI experiments.

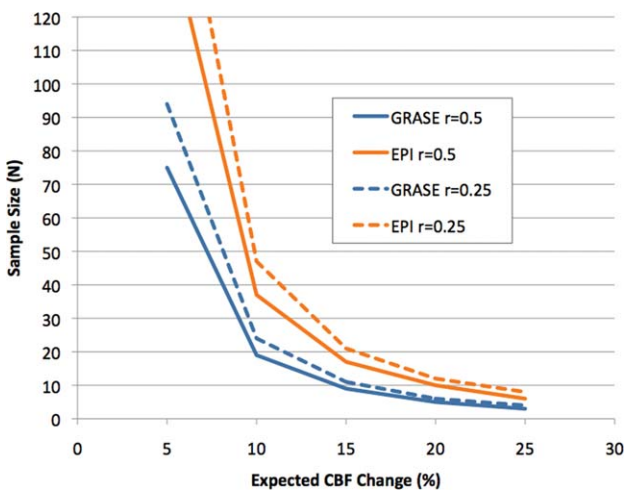

Figure 6. Sample size for a within-subject design including one baseline and one follow-up measurement for GRASE and EPI pCASL, respectively, with an assumed correlation coefficient of 0.25–0.5 between repeated measures ($\alpha = 0.05$ two-sided and power = 90%).

to preserve the point-spread function of 3D GRASE (25). Both segmented 3D GRASE with improved motion resistance and VFA approaches are actively being pursued in our laboratory.

The use of BS in 3D GRASE pCASL caused approximately 10% reduction in the labeling efficiency, given that the efficiency of each of the 2 nonselective inversion pulses was 95%. Using the calibrated labeling efficiency of 0.77, the absolute CBF values of whole brain match closely between GRASE (45.2 ± 8.99 mL/100 g/min) and EPI pCASL (47.8±9.20 mL/100 g/min). This result is consistent with previous studies on the efficiency of BS (19), and supports that BS can be reliably applied for quantitative perfusion imaging using pCASL.

Various imaging modalities have been used to study AD. Morphometric, perfusion, metabolic, and more recently, functional connectivity and amyloid imaging data have furthered our understanding of the disease development and progression. In the clinical setting, structural MRI, FDG-PET, and SPECT perfusion imaging have been routinely used to help with diagnosis. Compared with amyloid PET imaging, which measures amyloid plaques, one of the earliest pathological changes in AD, and structural MRI, which visualizes atrophy, a relatively late change in AD, the value of ASL perfusion MRI lies in that perfusion closely correlates with disease progression from MCI to AD, and therefore may serve as an imaging marker for therapeutic efficacy in clinical trials. For such purposes, quantitative MRI methods have unique advantages over FDG-PET which is not suitable for frequent scanning given required exposure to radioactivity. Establishing the longitudinal reliability and accuracy of these MRI methods is key to realize these advantages. The high longitudinal reliability of 3D GRASE pCASL demonstrated in the present study supports its use as a reliable measure of perfusion in MCI and AD patients.

There are several limitations of this study. First, the sample size is relatively small and may not represent an optimal sample of the MCI and AD population. Regression analysis of perfusion with behavioral assessments or clinical diagnosis was not feasible given that there was only one AD subject. Second, arterial sampling was not performed during the PET scan and, therefore, only relative CBF was obtained in the current 15O-water PET experiment. This is the reason that we chose to compare the spatial pattern of ASL CBF and PET rCBF maps using correlation analyses in individual subjects. Finally, the test–retest variability of pCASL was higher than those of automatic segmentation of structural MRI (~4.3%) (26) and amyloid PET (≤ 10%) (27,28). Compared with ASL repeatability studies performed on young healthy adults 1 week apart (14) and on six elderly subjects during the same scanning session (15) (ICC range, 0.8–0.95), the ICC values of the present study were lower (range, 0.4–0.8). This may be attributed to the challenges of ASL imaging in elderly populations (e.g., reduced CBF and prolonged arterial transit time) as well as the longer interval (~4 weeks) between repeated scans in the present study. Nevertheless, our sample size estimation indicated that approximately 10 subjects are needed for detecting a 15% CBF change with 90% power using 3D GRASE pCASL.

In conclusion, pCASL perfusion MRI with 3D BS GRASE readout is a promising imaging tool for the evaluation of MCI and AD. Further technical developments are needed for minimizing spatial blurring in 3D acquisitions.

REFERENCES

1. Jack CR Jr, Lowe VJ, Weigand SD, et al. Serial PIB and MRI in normal, mild cognitive impairment and Alzheimer's disease: implications for sequence of pathological events in Alzheimer's disease. Brain 2009;132(Pt 5):1355–1365.
2. Rabinovici GD, Jagust WJ. Amyloid imaging in aging and dementia: testing the amyloid hypothesis in vivo. Behav Neurol 2009;21:117–128.
3. Frisoni GB, Fox NC, Jack CR Jr, Scheltens P, Thompson PM. The clinical use of structural MRI in Alzheimer disease. Nat Rev Neurol 2010;6:67–77.
4. Alsop DC, Dai W, Grossman M, Detre JA. Arterial spin labeling blood flow MRI: its role in the early characterization of Alzheimer's disease. J Alzheimers Dis 2010;20:871–880.
5. Wang J, Aguirre GK, Kimberg DY, Roc AC, Li L, Detre JA. Arterial spin labeling perfusion fMRI with very low task frequency. Magn Reson Med 2003;49:796–802.
6. Floyd TF, Ratcliffe SJ, Wang J, Resch B, Detre JA. Precision of the CASL-perfusion MRI technique: global and regional cerebral blood flow within vascular territories at one hour and one week. J Magn Reson Imaging 2003;18:649–655.
7. Alsop DC, Detre JA, Grossman M. Assessment of cerebral blood flow in Alzheimer's disease by spin-labeled magnetic resonance imaging. Ann Neurol 2000;47:93–100.
8. Johnson NA, Jahng GH, Weiner MW, et al. Pattern of cerebral hypoperfusion in Alzheimer disease and mild cognitive impairment measured with arterial spin-labeling MR imaging: initial experience. Radiology 2005;234:851–859.
9. Dai W, Lopez OL, Carmichael OT, Becker JT, Kuller LH, Gach HM. Mild cognitive impairment and alzheimer disease: patterns of altered cerebral blood flow at MR imaging. Radiology 2009;250:856–866.
10. Raji CA, Lee C, Lopez OL, et al. Initial experience in using continuous arterial spin-labeled MR imaging for early detection of Alzheimer disease. AJNR Am J Neuroradiol 2010;31:847–855.
11. Alsop DC, Casement M, de Bazelaire C, Fong T, Press DZ. Hippocampal hyperperfusion in Alzheimer's disease. Neuroimage 2008;42:1267–1274.
12. Parkes LM, Rashid W, Chard DT, Tofts PS. Normal cerebral perfusion measurements using arterial spin labeling: reproducibility, stability, and age and gender effects. Magn Reson Med 2004;51:736–743.
13. Wang Y, Saykin AJ, Pfeuffer J, et al. Regional reproducibility of pulsed arterial spin labeling perfusion imaging at 3T. Neuroimage 2011;54:1188–1195.
14. Murphy K, Harris AD, Diukova A, et al. Pulsed arterial spin labeling perfusion imaging at 3 T: estimating the number of subjects required in common designs of clinical trials. Magn Reson Imaging 2011;29:1382–1389.
15. Xu G, Rowley HA, Wu G, et al. Reliability and precision of pseudo-continuous arterial spin labeling perfusion MRI on 3.0 T and comparison with (15)O-water PET in elderly subjects at risk for Alzheimer's disease. NMR Biomed 2010;23:286–293.
16. Fernandez-Seara MA, Edlow BL, Hoang A, Wang J, Feinberg DA, Detre JA. Minimizing acquisition time of arterial spin labeling at 3T. Magn Reson Med 2008;59:1467–1471.
17. Dai W, Garcia D, de Bazelaire C, Alsop DC. Continuous flow-driven inversion for arterial spin labeling using pulsed radio frequency and gradient fields. Magn Reson Med 2008;60:1488–1497.
18. Wu WC, Fernandez-Seara M, Detre JA, Wehrli FW, Wang J. A theoretical and experimental investigation of the tagging efficiency of pseudocontinuous arterial spin labeling. Magn Reson Med 2007;58:1020–1027.

19. Garcia DM, Duhamel G, Alsop DC. Efficiency of inversion pulses for background suppressed arterial spin labeling. Magn Reson Med 2005;54:366–372.
20. Chalela JA, Alsop DC, Gonzalez-Atavalez JB, Maldjian JA, Kasner SE, Detre JA. Magnetic resonance perfusion imaging in acute ischemic stroke using continuous arterial spin labeling. Stroke 2000;31:680–687.
21. Tzourio-Mazoyer N, Landeau B, Papathanassiou D, et al. Automated anatomical labeling of activations in SPM using a macroscopic anatomical parcellation of the MNI MRI single-subject brain. Neuroimage 2002;15:273–289.
22. Fernandez-Seara MA, Wang Z, Wang J, et al. Continuous arterial spin labeling perfusion measurements using single shot 3D GRASE at 3T. Magn Rason Med 2005;54:1241–1247.
23. Liang X, Tournier J-D, Masterton R, Connelly A, Calamante F. A k-space sharing 3D GRASE pseudocontinuous ASL method for whole-brain resting-state functional connectivity. Int J Imaging Syst Technol 2012;22:37–43.
24. Wang DJ, Alger JR, Qiao JX, et al. The value of arterial spin-labeled perfusion imaging in acute ischemic stroke: comparison with dynamic susceptibility contrast-enhanced MRI. Stroke 2012;43:1018–1024.
25. Hennig J, Weigel M, Scheffler K. Multiecho sequences with variable refocusing flip angles: optimization of signal behavior using smooth transitions between pseudo steady states (TRAPS). Magn Reson Med 2003;49:527–535.
26. Jovicich J, Czanner S, Han X, et al. MRI-derived measurements of human subcortical, ventricular and intracranial brain volumes: reliability effects of scan sessions, acquisition sequences, data analyses, scanner upgrade, scanner vendors and field strengths. Neuroimage 2009;46:177–192.
27. Tolboom N, Yaqub M, Boellaard R, et al. Test-retest variability of quantitative [11C]PIB studies in Alzheimer's disease. Eur J Nucl Med Mol Imaging 2009;36:1629–1638.
28. Joshi AD, Pontecorvo MJ, Clark CM, et al. Performance characteristics of amyloid PET with florbetapir F 18 in patients with alzheimer's disease and cognitively normal subjects. J Nucl Med 2012;53:378–384.